Dust plasma crystals

Blaž Kmetec
Faculty of Mathematics and Physics, University of Ljubljana

Supervisor: **Dr. Milan Čerček**
Institute Jožef Stefan,Section F8, Plasma laboratory

March 23, 2002

Contents

Abstract

The creation and examination of the dust plasma crystal under certain experimental manners is considered. Questions concerning dust self-organization and special properties of the melting phase transition are presented. The particular attractivity of phase transition investigations lies in the fact that the motion of each individual lattice dust particle can be directly observed.

1 Introduction

It is well known that matter changes from a solid to a liquid to a gas as the temperature is raised. At even higher temperatures the plasma state is reached - a hot gaseous mixture of ions and electrons in which the particles swirl about at incredible speeds, and which can only be tamed by electrical and magnetic fields.

We have learned that the solid-liquid-gas-plasma sequence expresses the increasing randomness and disorder of the particles' behaviour. Therefore, a common sense would suggest that solidification in the plasma state would be as unlikely as the survival of an ice cube on a red-hot stove. This view, however, is altered with the emergence of phenomena such as self-organization and pattern formation in non-equilibrium plasmas.

One example of such ordering phenomena is the observation of a remarkable stable lattice structure formed by micron-sized dust grains added to a plasma. We will refer to such structure as a "plasma crystal" because of its periodicity. In contrast to atomic solid-state crystals the macroscopic structure is clearly vivid, hopefully contributing to the theory of general properties of crystalline state in simple and easy-to-control manner.

Although melting and freezing are two of the most common structural phase transition in everyday experience, surprisingly little is known about their microscopic mechanisms. Part of the difficulty in crafting a complete understanding of such fundamental transformations is that experiments on conventional materials, such as copper or water, can tell us very little about what happens on the atomic scale as a crystal transforms itself into a fluid. Not only are atoms small and moving rapidly, but comparatively few of them take part in the process in any one time. Even computer simulations are hard-pressed to accommodate the enormous sample sizes and the range of timescales involved in converting a chunk of ice into a puddle of water.

The melting of dust plasma crystals is the transition where the long-range order of the crystal starts to deteriorate due to thermal excitations. The general characteristics of crystal melting are still not entirely understood, and plasma scientists believe that examinations of plasma crystal melting, especially in two dimensions, can allow us deeper insight into the picturesque and mysterious world of phases of matter.

In our previous essay [1] we introduced dust grains in plasma. Let us summarize basic dusty plasma principles first and then consider dust formation in cold (laboratory) plasmas.

1.1 Quick overview of dusty plasmas

Dusty plasma physics is a rapidly developing research being stimulated by technical applications, the discovery of the plasma crystals, astrophysical applications and by fundamental science issues including self-organization processes.

In space, dusty plasmas are ubiquitous, including interstellar clouds, circumstellar and protoplanetary accretion disks, nova ejecta, and planetary magnetospheres. The thermodynamics, chemistry, and electromagnetic evolution of these systems are affected and sometimes dominated by dust. In microelectronics fabrication, particles can grow in the plasmas in surface processing reactors, and remain electrically suspended until they fall to a surface and contaminate it, Thus it is not surprising that astronomers and industrial researches have investigated many physical processes, including especially the problem of dust charging. Usually the dust is negatively charged due to higher electron mobility and therefore current. For a plasma with an electron temperature of a few electronvolts, a micrometer-sized dust particle can be charged up to about 10^4 electrons.

For spherical dust particle of size a (dust particles are nanometer to micrometer size), the surface potential is typically of the form of the screened coulomb potential - well known Debye-Hückel potential:

$$V(r) = V(a)\frac{a}{r}\exp -(r-a)/\lambda_D, \tag{1}$$

where λ_D is Debye length, calculated from the ion and electron Debye lengths:

$$\frac{1}{\lambda_D^2} = \frac{1}{\lambda_{De}^2} + \frac{1}{\lambda_{Di}^2}; \tag{2}$$

$$\lambda_{De,i} = \sqrt{\frac{\epsilon_0 k T_{e,i}}{e^2 n_\infty}}; \tag{3}$$

The balance between the electrostatic potential and the energy from random agitation, the later, at the molecular level, arising mostly from the kinetic energy of ions, is conventionally measured by a *coupling parameter*

$$\Gamma = \frac{Z_d^2 e^2}{4\pi\epsilon_0 k d T_d}\exp -d/\lambda_D, \tag{4}$$

which is simply the ratio of the coulomb energy between two neighboring particles, separated by a distance d, to their kinetic energy kT_d. In many dusty plasmas, the coupling parameter can be of the order of unity and often much larger. These dusty plasmas are strongly coupled and can arrange themselves into structures as dust clouds, droplets or crystals. Simple Monte-Carlo simulations suggest that the critical coupling parameter - the value where crystallization takes place - is $\Gamma_C = 172$.

The physics of plasma crystallization is the unique bridge connecting the fields of (nonideal) plasmas and condensed matter physics. Dust plasma crystal is formed by the mutual electrostatic repulsion of particles of dust held within an ionized plasma. Colloidal suspensions, i.e., charged particles immersed in an aqueous solution, provide a similar physical system in which crystallization was studied. In this essay, only dust plasma crystallization will be considered, although we will make some comparison in the last chapter.

The forces controlling the structure and thermodynamics of plasma crystals are coulomb forces and neutral gas friction, which cools the particles down to brownian motion. Experimental conditions for crystallization thus require a partially ionized plasma with a low (room) temperature neutral gas component and dense dust component. Such conditions can be produced easily in low-power radiofrequency discharges.

The reader may wish to read introductory articles concerning plasma dust crystals; in that case, the reader may refer to, for example, [2, 3, 4, 5]. For detailed discussion and topics (or references) not found in this essay, see for example [6].

2 Observations and modeling of crystal structures and crystal melting

2.1 New phase state

The seed is planted: first concepts. The conditions for solidification are given.

As the secondary emission and photoemission can be neglected in the laboratory dusty plasma, the dust particle in plasma is charged negatively because of higher electron mobility (the problem is, to the first approximation, simply the scattering on a coulomb potential, see [1, 7, 8]). In many laboratory experiments, clouds of micrometre-sized particles are trapped in an ion sheath between the plasma and an electrode. While the electrons follow the radiofrequency electrical field, the ions and microparticles, because of their large inertia, are only reacting to the time-averaged field, which generates the levitating electric force. The distribution of the net ion space charge in the sheath is sufficiently homogeneous, which implies that the electric field increases nearly linearly from the plasma edge to the electrode. This leads to vertical confinement of the particles in an effective parabolic potential energy well [7], at least for small amplitudes of particles' oscillations.

The particle clouds that sediment towards the lower electrode require a lateral confinement to prevent the unrestricted radial expansion under the mutual repulsion of the particles. Here one can distinguish two types of confinement. In "surface confinement", a flat metal ring on the electrode or a depression of the electrode surface is used to raise the equipotentials at the boundary of the cloud and to produce a localized radial electrical field that balances the electrostatic pressure of the cloud. In "volume confinement", a shaped electrode is used to produce a parabolic potential well $V_{pot}(r) = \frac{1}{2}\gamma r^2$. Besides using the distortion of the equipotentials for particle confinement, the discharge mechanism can form regions of enhanced positive potential plasma above sharp edges of the electrode, in which negative microparticles are trapped.

Inhomogeneous charge distributions on the surface of the microparticles were originally discussed in connection with the formation of electric dipoles that could lead to additional attractive forces, for instance in the coagulation processes of dust particles. For rod-shaped objects the role of inhomogeneous charge distribution becomes even more important. However, in laboratory experiments particles are usually already prepared as non-insulating spheres and externally injected or chemically synthesized in discharges so that they preserve their spherical shape and surface charge homogeneity. In space, conditions are far more complicate as in laboratory experiments.

First theoretical predictions and conditions for solidification in dusty plasma were developed in 1985 by Ikezi [9] on the basis of the Wigner's theory of Coulomb solids. Here the dust charge q, needed for the

calculation of the shielded coupling parameter

$$\Gamma_S = \frac{q^2}{4\pi\epsilon_0 k d T_d} \exp(-d/\lambda_D),$$

is calculated from the equilibrium (floating) potential of the dust particle. The expression for the floating potential is, according to standard plasma textbooks (see for example, [10, 8]), $V(a) = (kT_e/2e)\ln(m_i/2\pi m_e)$.

If the assumption of dust particle being negatively charged and its size being smaller than the Debye length, $a < \lambda_D$, is employed, the potential of the particle is approximately $q/4\pi\epsilon_0 a$. This potential should be equal to the floating potential and we have an approximate expression for charge

$$q = q1 = (2\pi\epsilon_0 a T_e/e)\ln(m_i/2\pi m_e). \tag{5}$$

This expression is valid only when $n > |q_1/e|N$ is satisfied; the difference between ion and electron densities equals $|q_1/e|N$. When this value is larger than the plasma density, there are no electrons available to charge the particles as much as q_1. Therefore, the charge of the particles should be

$$q = q_2 = en/N. \tag{6}$$

In other words, the system consists of negatively charged particles and positive ions of density n.

By combining

$$\Gamma_S > \Gamma_C \tag{7}$$

with the expression of q given by either Eqs. (5) or (6), depending on the relation between n and N, a range of n and N where solidification takes place can be found. An example of such a range is shown in Fig. 1. The dotted line indicates $\Gamma_S = \Gamma_C$ when $q = q2$. The solid lines are obtained when q equals $q1$ which depends on a. The solidification condition is satisfied in the regions enclosed by dotted and solid lines. The lattice melts at the boundary of the area.

There are three different reasons why this occurs depending on the segment of boundaries A-B, B-C, and C-A labeled in Fig. 1. The segment A-B is approximately given by $\Gamma = \Gamma_C$ with $q = q1$ given by Eq. (5). The reduction of coulomb energy caused by the increase of interparticle distance causes melting (the higher the dust particle density, the higher the coupling parameter; above A-B line - the point B crosses $q1 = q$, i.e. $n/N = q1/e$ - there is a non-solid state). On segment B-C, the Debye screening reduces the coulomb interaction (the lower the plasma ion density, the higher the screening length and hence higher coupling). The melting on the segment C-A is caused by the reduction of q because q decreases upon the reduction of plasma density. This segment is approximately expressed by a combination of $\Gamma = \Gamma_C$ and Eq. (6).

In the case of laboratory plasma, a partially ionized plasma having parameters of $T_e = 3eV$ and $n = 10^7 - 10^{10} cm^{-3}$ can be produced easily in a neutral gas density of $n_n = 10^{12} - 10^{13} cm{-}3$. The plasma is produced by the impact ionization of neutral gas by the electrons injected from the hot filaments or by the electrical field. If small particles are introduced into such plasma, the temperature of the particle equals the neutral gas temperature, which is room temperature, because the particle-neutral gas relaxation time is much shorter than the particle-electron relaxation time. In a case of argon plasma, for example, Eq. (5) gives $q = 36000e$ when $a = 3\mu$m . Since the plasma container, which is at the floating potential, is negative with respect to the plasma potential, the particles are confined electrostatically.

The particle crystal can be observed in the laboratory plasmas using both optical microscopy or light scattering.

2.2 Birth of the crystal

Dust crystals are observed experimentally for the first time. The simple experimental arrangement promises further progress. The striking optical visibility offers new routes to

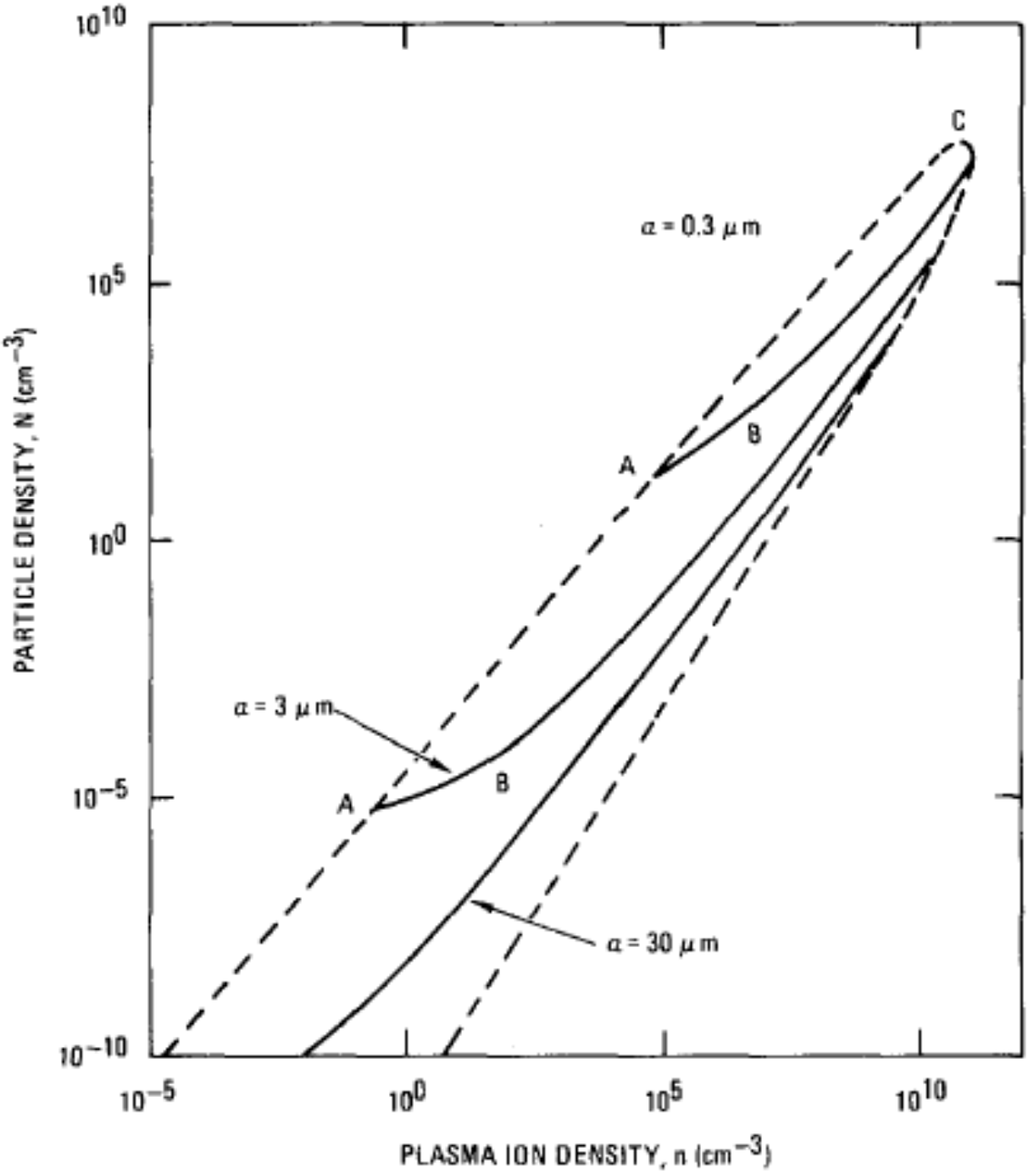

Figure 1: A range of plasma density n and dust particle density N where a coulomb solid is formed when $T_e = 3eV, T_i = 0.03eV$, and $m_i/m_e = 400 \cdot 1800 = 720000$. After [9].

crystal research.

Max Planck Institute for Extraterrestrial Physics

First experimental observations of dust crystals were reported in 1994 by a group of six people [11], five from Germany [1] and one from the university of Iowa in the United States. The simple experimental arrangement is the foundation of all of the following experiments (Fig. 2).

The plasma is made from argon gas enclosed in a small vacuum chamber and excited by a radio-frequency discharge. The chamber also contains two electrodes, a lower circular electrode 8 cm in diameter and an upper electrode in the form of a ring - a 10-cm circle in which a 3-cm hole has been cut. Both electrodes

[1] Max-Planck Institute für Extraterrestiche Physik, 85740 Garching, Germany

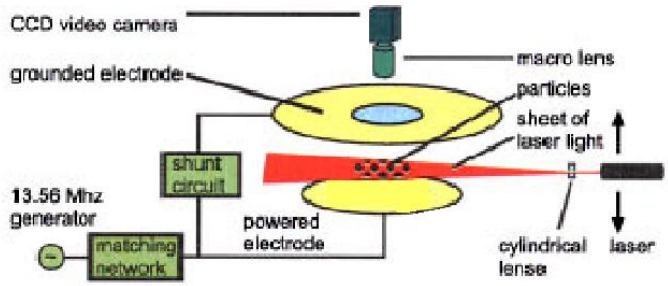

Figure 2: Experimental scheme. A vacuum vessel that encloses the electrode assembly is not shown. From [11].

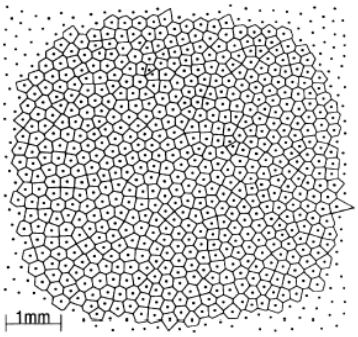

Figure 3: Wigner-Seitz analysis of particle location from the image of the particle cloud. From [11].

are arranged horizontally and are 2 cm apart.

For dust, a few milligrams (that is approx. 100 000 units) of 7 μm in diameter nearly identical ($\pm$ 0.2 μm size distribution; less fluctuations in particle size, stable the crystal system) plastic (melamine/formaldehyde) spheres are places in a sieve above the hole in the upper electrode. This is agitated to release particles into the plasma.

In the conditions of the experiment, the plastic spheres form a disk-shaped cloud some 3 cm in diameter, levitated above the center of the lower electrode, near the sheath boundary. Particles are organized in approximately 18 planar layers parallel to the electrode, the structure with 0.5 mm cell size being visible to the naked eye. Remembering the total number of particles is about 100 000, the extend in both lateral direction is 60-70 cells.

Observations are made by illuminating a plane with a sheet of HeNe laser light, with a thickness of 100 $\pm$ 23 μm and a breadth of 2 cm. Such a fan-shaped laser beam is made by putting a cylindrical lens in front of a laser. The scattered light is recorded with a CCD video camera through a hole in the top electrode. The positions of the particles within each layer are determined simply by shifting the laser beam vertically.

The explanation is straightforward. The lower electrode acquires a negative electrical bias of 14V, which is enough to levitate (negatively charged) dust particles. Because of their mutual repulsion, the charged grains seek a minimum of total energy by forming an ordered structure. Levitation is accomplished when an upward repulsive electric force arises from the repulsion between the negatively charged grains and the lower discharge electrode, and balances the weight of the dust grains.

Because the container with its fields prevents dust particles from moving apart indefinitely, the spheres adopt a configuration which minimizes their total energy, given their temperature and density. If the charge-mediated interaction between the spheres is great enough to overcome the buffeting of the surrounding gas, then they form into regularly spaced arrays. If the thermal energy of the gas wins, the plasma crystal melts into a dynamic and disordered state reminiscent of a fluid.

In the lattice more than 60% of the cells are hexagonal with 0.25 mm between nearest neighbors. The other cells are either five- or seven-sided. Although this increase of order hints at the solid phase of the plasma crystal, a local hexagonal structure is also well known in liquids. It is the regularity of Wigner-Seitz cells (which are nowadays computed with ease) than implies the solid state. The spectator who undertakes the fantastic voyage into this atomic scale world is immediately intrigued by the beauty of this regular pattern formed by the grains (Fig. 3). The crystal is stable for hours, except for small, spontaneous rearrangements of individual particles that occur every few seconds. Moreover, the trembling of individual grains, due to Brownian motion about their equilibrium positions, is both visible and measurable.

The number of elementary charges on the dust grain is estimated to be in a range between 9800 and

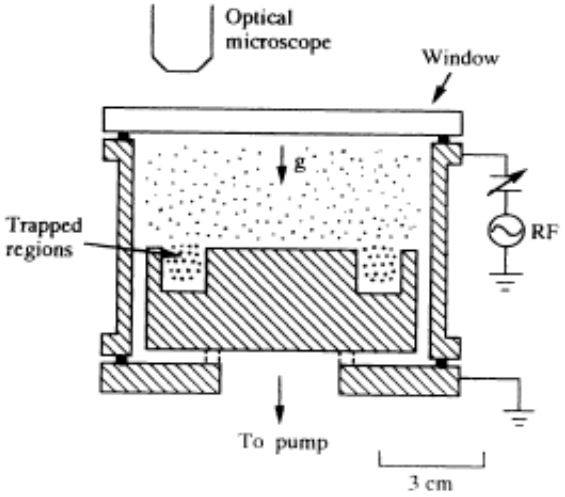

Figure 4: Sketch of the side view of the cylindrical discharge system. From [12].

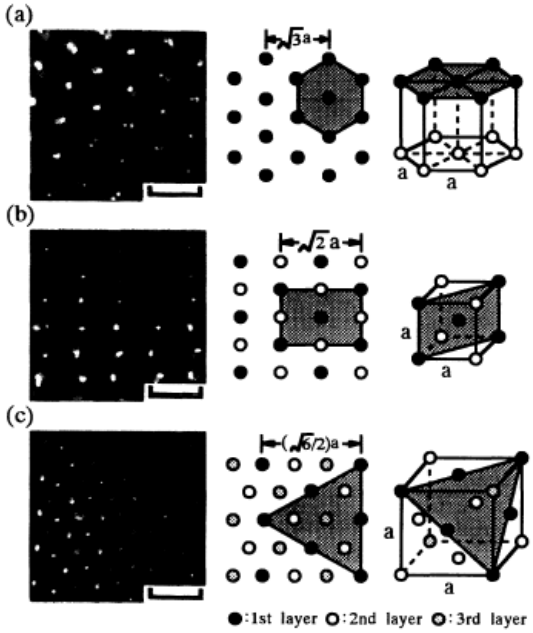

FIG. 3. Micrographs and sketches of the different crystal structures. (a) Hexagonal; (b) bcc; (c) fcc. The center column corresponds to the structures in the micrographs. The graded areas in the sketches are normal to the optical axis. The bars correspond to 200 μm.

27000. In order to estimate the coupling parameter Γ we need to know the particles' kinetic energy also. The particles are cooled by the neutral gas. Based on frame-by-frame measurements of the mean particle velocity, the particle kinetic temperature is calculated to be $T_d = 310K$, which is close to room temperature. The coupling parameter is then resulting in value higher than 20700, which is quite higher than its critical value.

The next steps are, evidently, investigation of the three-dimensional properties of the crystal, and elaborate observations of melting.

2.3 The observations develop rapidly

Different structures and their coexistence are created. Plastic spheres are substituted with $Si0_2$: it is metals and silicates that are relevant to plasma processing and astrophysics. Optical microscope is used for the first time for coulomb crystal investigations.
Chungli University group[2], 1994

The experiment, its report [12] almost immediately following the previous one, is conducted in a cylindrical symmetric plasma system. Figure 4 shows the side view of the system. It consists of a hollow outer electrode, a grounded centre electrode with a ring-shape groove on the top for particle trapping, and a top glass window for observation. The system is pumped by a diffusion pump. O_2 and SiH_4 are introduced into the chamber with background argon gas. The particle size and number density increase with the reactive gas flow on-time and pressure. After the formation of micron size particles, the reactive gas flow is turned off. Particles can be very well trapped in the toroidal groove. Under the gravitational force, the particle diameter slowly increases with the decreasing height. The precisely controlled discharge power is the main control parameter. A digital video recording system is used to monitor the image of the particles illuminated by a HeNe laser through an optical microscope mounted on the top of the chamber. The optical axis is parallel to the symmetry axis of the system.

[2]National Central University, Chungli, Taiwan 32054, Republic of China

With decreasing the discharge power, the formation of different crystals is observed in the groove region. The structure is stationary except the small fluctuations around the equilibrium positions.

Hexagonal structure (also hcp) is easily observed, as well as bcc and fcc structures. See Fig. 2.3 For example, in the bcc structure (2.3b) the lattice constant is about 200 μm which is also about $\sqrt{2}$ times the distance between the two horizontal planes. Its direction is (100) along the optical axis. The fcc structure (2.3c) has the (111) direction pointing along the optical axis.

Beside various defects, coexisting domains with different crystal structures are observed, for example, the coexistence of bcc and fcc structures. The domain boundary moves with constant speed. Increasing the discharge power again causes the melting of the crystal.

2.4 Charge measurement

In order to get more accurate value of the coupling parameter, the dust charge q has to be precisely measured. The theoretical determination of the dust charge in the sheath region is very complicated since electron and ion distribution function have to be known. The dust component in plasma cannot always be considered as a weak perturbation to a preliminary prepared plasma, and an increase in dust density should decrease the charge on the dust particles as particles would screen the plasma fluxes to the other dust particles in strongly correlated dusty plasma. Moreover, the presence of electrostatic fluctuations and turbulence can further increase the complexity of dust charging. It is therefore necessary to measure the charge directly in the plasma.

In the experiment of the Kiel University group [13], dust particles in discharge are suspended in the sheath of the lower electrode where the upward force $F_e = qE$ balances the weight $F_g = m_d g$ of the particle. It is possible to excite resonant oscillations of the particle in this potential well, by modulating the radiofrequency discharge voltage with a small low-frequency voltage.

The modulation technique is based on the oscillation of the particle in the effective potential well. For this purpose a small additional low-frequency voltage is applied that exerts a periodic force on the particulates. Plasma densities and temperatures are assumed not to be affected by this modulation. The behaviour of the grain can be described by the equation of a motion for a driven damped oscillator:

$$M\ddot{x} = qE(x,t) - m_d g - m_d \beta \dot{x}. \tag{8}$$

x measures the position of the particle above the lower electrode. The electric field $E(x,t)$ is slowly time varying because of the modulation. The damping constant β is related to the neutral drag force.

It is justified to assume a linear increase of $E(x)$ in the vicinity of the particles' equilibrium position. Then the potential will be sufficiently parabolic and consequently the oscillations harmonic.

Varying the direct current electrode bias voltage sinusoidally with small amplitudes one can also modulate the electric field sinusoidally

$$E(x,t) = e(x_0) + (x - x_0)E' + \Delta E \sin(\omega t), \tag{9}$$

where the spatial electric field variation is related to the averaged space charge $n_i e$ through Poisson's equation:

$$dE(x)/dx = E' = -n_i e/\epsilon_0. \tag{10}$$

Inserting Eq. (9) into Eq. (8) yields the following asymptotic solution:

$$x(t) = x_0 + AR(\omega)\sin(\omega t + \varphi) \tag{11}$$

Figure 5: Experimental arrangement from [13].

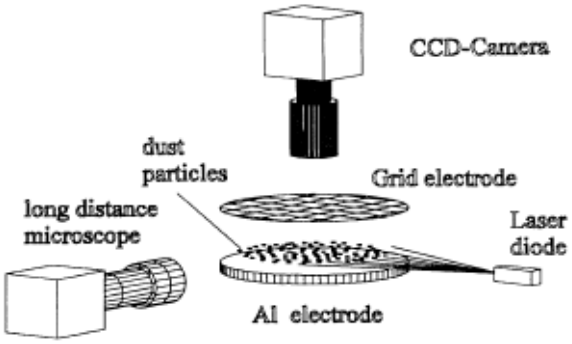

where x_0 describes the equilibrium position with $qE(x_0) = m_d g$ (similar to Millikan's historical experiment). The amplitude $AR(\omega)$ consists of a constant factor A and the frequency dependent response function

$$R(\omega) = [(\omega_0^2 - \omega^2)^2 + \beta^2\omega^2]^{-1/2}. \tag{12}$$

The resonance frequency is given by

$$\omega_0^2 = \frac{qn_i e}{\epsilon_0 m_d}. \tag{13}$$

The modulation technique is described in terms of a single particle. Particles, however, are strongly coupled. In order to resolve this apparent contradiction we recollect the property of a harmonic potential well that the resonance frequency is independent of the position in this well. So, if we have a crystal with a few layers thickness in this well the crystal as a whole should oscillate with the resonance frequency. Furthermore through the strong coupling of the dust grains the crystal behaves like a rigid body. It has been confirmed experimentally that particles in different layers show the same amplitudes, keep their distances and all have the same resonance frequency.

2.5 Destroying the order

Improved approach to dust charge measurement is introduced. Vertically aligned structure is favoured over close packed in a flat 2D crystal. Melting can be induced in two different ways. In any case, the cause is the increase of oscillations and the thermal motion of crystal particles.
Kiel University group [3][13]

Melting

The improved charge measurement allows more precise information and control over the system. Experimental design is somehow similar to the one from the Max Planck group (Fig. 5). Melamine-formaldehyde spheres of 9.4μm in diameter are used in a parallel plate discharge, operated in helium. The discharge consists of a lower, powered aluminum electrode of 15 cm in diameter and an upper grounded grid mesh electrode of approximately 1 cm in mesh size. The discharge gap is 6 cm wide. The electrodes are placed in a vacuum chamber with four horizontal and one top viewport. The dust is contained in a dust dropper within the vacuum vessel above the upper electrode. The particles are illuminated by a horizontally expanded thin sheet of laser light and are viewed in scattered light with a CCD camera from top through the grid electrode.

[3]Institut für Experimentalphysik, Christian-Albrechts-Universitat,24098 Kiel, Germany

A second HeNe laser is vertically expanded to illuminate a cross section of the crystal in order to measure the resonance of the particle and to investigate the layer structure of the crystal. Through a side window the particles are observed by a second video camera.

The melting transition can be induced in two ways, either by raising the rf power or by reducing the pressure [4]. The transition is monitored by a video camera and quantitatively analyzed by means of correlational functions. Two dimensional plasma crystals with two or more layers are found to undergo these transitions. The higher the number of layers the more disordered the whole crystal. Moreover, the layers nearest the electrode melt first and show more violent particle motion, while the uppermost layer stays solid longest.

- Melting by reducing the gas pressure

  Gas pressure is reduced from 118 to 39 Pa, while the discharge power is kept fixed, as well as the amount of dust particles that was inserted at the beginning of the experiment. A Wigner-Seitz analysis yields that 91.5% of cells are hexagons with almost having the same size, others are again five- or seven-sided. The positional order is maintained for at least five nearest-neighbour distances. The particles of the lower layer are located exactly below a particle of the higher layer. This vertically aligned arrangement is apparently not a minimum energy configuration if one considers only coulomb interaction of the particles. We will consider vertical alignment of the particles later.

  To investigate the dynamics of the particles during the melting transition the trajectories of individual particles are recordered. For this purpose, a series of 11 snapshots of the dust particles are taken at 1s intervals. The results show that at 188Pa most of the particles do not move but stay in their individual Wigner-Seitz cells. Only at the edges there is some particle motion observable. At a pressure of 86Pa there are some regions where the particles stay in their initial positions and in other regions the particles move along streamlines at the boundary of the crystalline regions. Note that the trajectories do not intersect, which is typical of fluid motion. The motion is further enhanced at 57Pa. Here streamlines are clearly observable, but there are some regions in which the particle motion becomes not aligned in streamlines. Finally, at 39Pa there is no ordered motion observable. The number of oscillating particles and the oscillation amplitude increases during pressure reduction.

  From the above results the dust particle arrangement is recognized as the solid state at pressures above 100Pa, as the fluid state below that value, and as a gaslike state at the lowest pressure values.

  With the measured values of the charge and kinetic velocity of dust particles the coupling parameter is obtained. In the solid state the values are found in the range 1000-2000. With reduced gas temperature Γ drops dramatically due to the higher dust temperature to the value 3 at 39Pa. The interpretation of the observed high dust temperature lays in the ion flux from the bulk plasma onto the electrode, which balances the energy loss due to dissipation of the oscillatory and erratic kinetic energy through friction with the neutral gas background.

- Melting by increasing the discharge power

  Increasing of discharge power from 10W to 60W at constant pressure 100Pa leads to melting of the dust crystal too, with the corresponding decreasing positional order, similar to pressure reduction induced melting. Here two differences from the melting by pressure reduction can be noticed. The first one is that the interparticle distance is decreasing from 480 μm at 10W to 340 μm at 60W.The other difference is that a gaslike state is not reached in this and in a further increased power range. The moving of the particle close together can be explained with decreasing Debye length due to increased ion density with power. High damping is the cause for less erratic motion at high discharge power. However, at the transition both the ion density and the interparticle distance are changing, leading to

[4] Other parameters could be varied, too - for example temperature; however the kinetic temperature is not easily independently controlled, since the plasma is not necessarily in thermal equilibrium

an almost constant screening strength. So here the particle oscillations and the so-enhanced particle temperature leads to the melting of the crystal too.

Vertical alignment

The vertical alignment of the particles in a flat crystal can be explained by nonreciprocal attractive forces on the particles due to ion streaming motion. These forces overcome the dust Coulomb repulsion. They are also responsible for particle oscillations.

In order to evaluate the forces by distortion of the ion trajectories, MC simulations of the experiment are carried out [14]. The system consists of two hexagonal layers of dust particles with the interparticle and vertical distances taken from the experiment (a=450 nm, d=360 nm). Charge-exchange collisions are also taken into account. From the ion trajectories the forces acting on the dust particle are calculated.

The results imply that the ion cloud of the upper particle provides an attractive force for the lower dust particles. See Fig. 6,7. This seems to be the reason for the alignment of the particles.

When the lower dust layer as a whole is shifted with respect to the upper layer, then the ion cloud is still found directly below the *upper* particle and is only slightly affected by the position of the lower particle layer. On the other hand, there is a strong restoring force on the lower provided by the ion cloud. These findings are the key points in the further discussion of the stability of this dust particle arrangement. The stability and the oscillations of the particles about their equilibrium positions can be studied analytically in a model consisting of interacting chains of masses and springs (see Fig. 8).

The main consequence of these studies is that undamped oscillations of the particles in the presence of the friction arise because of available free energy that comes from the streaming ions, which create the ion cloud below the upper particle and attracts the lower particles. The aligned structure is energetically favoured over hcp structure because of the nonreciprocal forces that reflect the symmetry breaking by streaming ions. These forces are also responsible for instabilities that lead to experimentally observed heating during the melting transition.

2.6 Phase diagram

Molecular dynamics (MD) simulations lead to precise phase diagram together with a triple point, connecting bcc, fcc and liquid state, in 1997

As the progress in modeling of crystallization with MD simulations on a basis of thermodynamic had increased, it became possible to construct a phase diagram, connecting a liquid and solid phase [17]. However, MC and MD simulations can handle only a finite number of particles in the direct pairwise summation of interparticle potential energies. in order to imitate a system with an infinite number of particles, one may apply periodic boundary conditions to the simulation volume. For a cubic simulation box of side length L, the effective pair potential becomes

$$\Phi_{eff}(r) = \Phi(|\vec{r}|) + \sum_{\vec{n}} \Phi(|\vec{r} + \vec{n}L|),$$

where $\Phi(|\vec{r}|)$ represents the interaction energy between two particles and all their periodic images. The sum over $\vec{n} = (l, m, n)$ represents the periodic images. With the assumption of the interparticle potential being of the Debye-Hückel type (1) the equations of motion

$$\frac{d\vec{r}_i}{dt^2} = -\sum_{j \neq i}^{N} \Delta\Phi(\vec{r}_i - \vec{r}_j), \quad i = 1, \ldots N \tag{14}$$

are integrated, with the number of particles N used for simulations are $N = 686$ for a bcc and $N = 500$ for a fcc lattice. These lattices are used as initial conditions, and the system is allowed to equilibriate to the desired Γ for some time before averaging its properties. In the model, long-range particle interactions are accurately accounted for over the entire range of cell sizes.

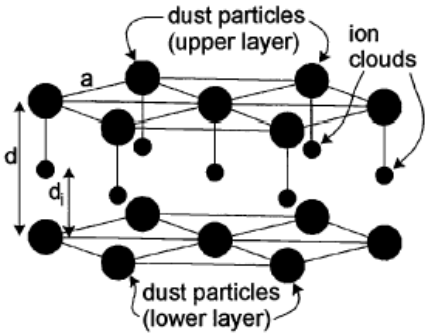

Figure 6: A single cell from the simulated bilayer system. From [15].

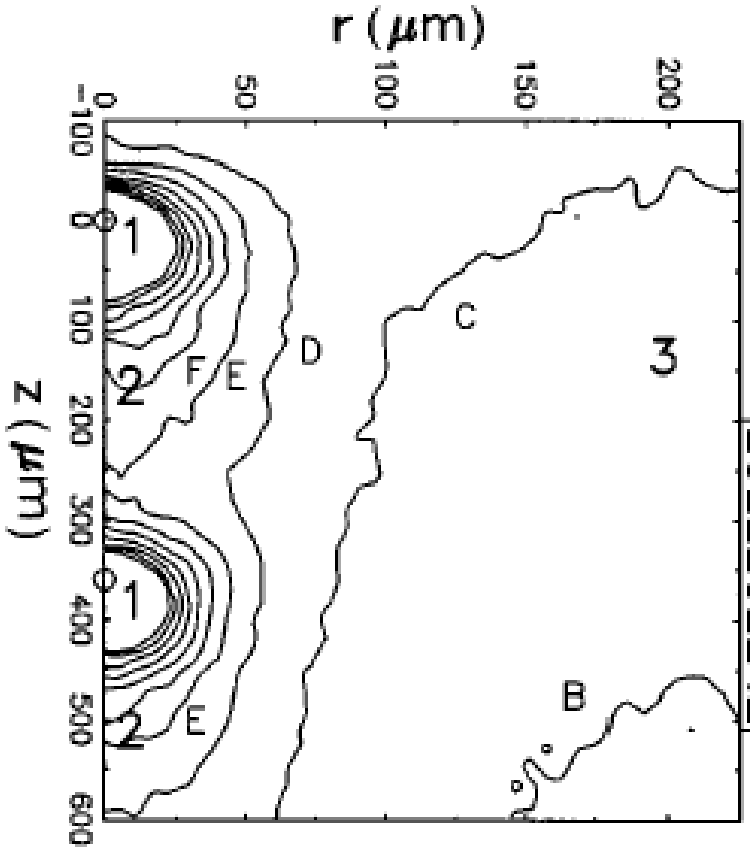

Figure 7: Relative (to the boundary) ion density distribution obtained from the MC simulations as a function of the parallel (r) and perpendicular (z) distance from the origin. One dust particle is placed in the origin ($r = 0, z = 0$), the other is 360 μm higher ($r = 0, z = 360\mu m$)). One can identify three different regions in this plot.For $r > 100\mu m$ there is an almost undisturbed region (region 3). Here the ion density slowly decreases with increasing z because of the ion acceleration by the electric field. Close to the dust particles (region 1) there is a very high ion density due to trapped ions in the potential well of the dust particles. Below the dust particles one can see a region (region 2) of enhanced ion density (ion cloud) with respect to the undisturbed ion density. It is formed by ions which are deflected by the attractive forces between dust particles and ions. The ion cloud of the upper particle provides an attractive force for the lower dust particles. This is the reason for the alignment of the particles. From [16]
.

Figure 8: The coupled chain model. Solving the equations of motion, the frequencies of oscillation are obtained and also a critical frequency of oscillation, where the crystal melts. See [16].

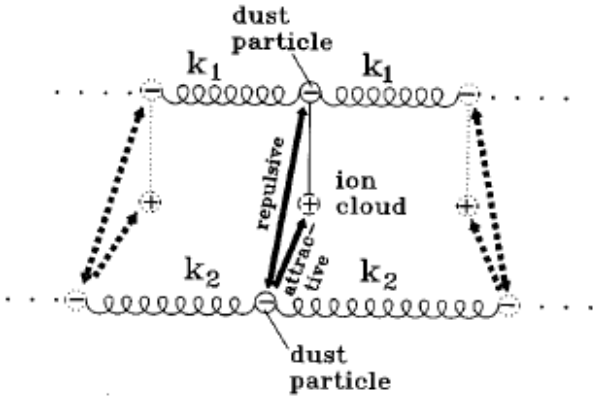

Figure 9: Phase diagram of Yukawa systems in the (κ, Γ) plane. From [17].

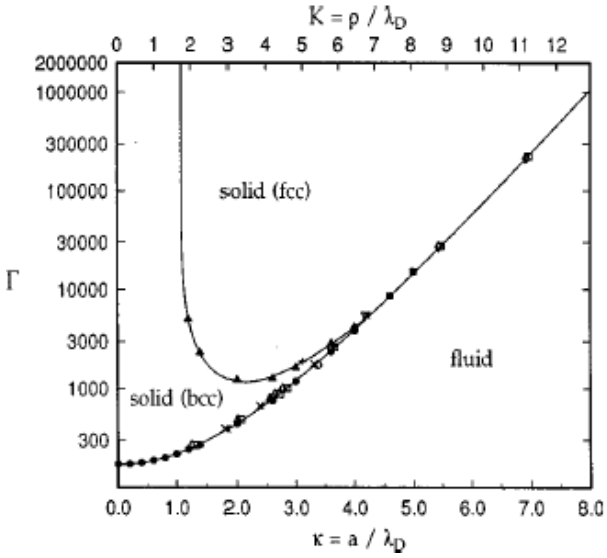

Performing the simulation, the dependence of Γ on the interparticle distance is obtained as the phase diagram, connecting two solid (fcc, bcc) phases and a fluid phase (Fig. 9). The weakly screened regime $0 \leq \kappa \leq 1$ (κ is the ratio of the Wigner-Seitz radius to the Debye length, $\kappa = a/\lambda_D, a = (3/4\pi n)^{1/3}$, n is the dust particle density). This fluid-solid phase transition, as well as the fcc-bcc transition is of the first order. The triple point is estimated to be $\kappa = 4.28$ and $\Gamma = 5.6 \cdot 10^3$.

These calculations still need the experimental support. As we will see immediately, phase transitions are quite more complex.

2.7 New phases reveal

Two states between ordered (crystalline) and disordered (liquid or gas) are described. Surprising changing of order may lead to perception of new intermediate states in melting transitions generally.

[11]

Further investigations of the phase transition revealed step-by-step flat dust crystal transition through four experimentally observed states. The experiment (with the same set-up as the first one) starts from the well-established crystalline state at 0.42mbar pressure. Transitions are followed by continuous lowering of

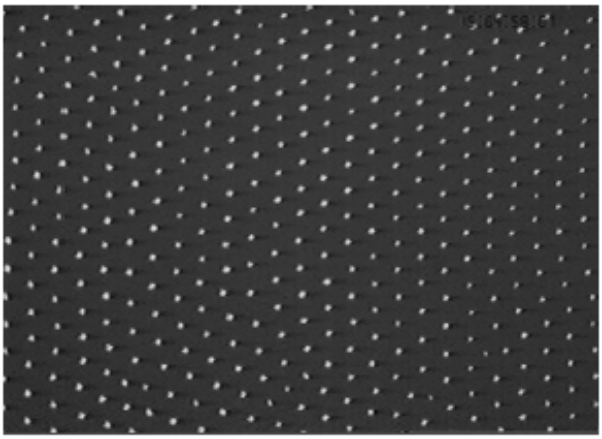

Figure 10: The CCD image of a horizontal lattice plane of a plasma crystal (top view). The area shown is $6.1 \times 4.2 mm^2$ and contains 392 particles of 6.9 μm diam.

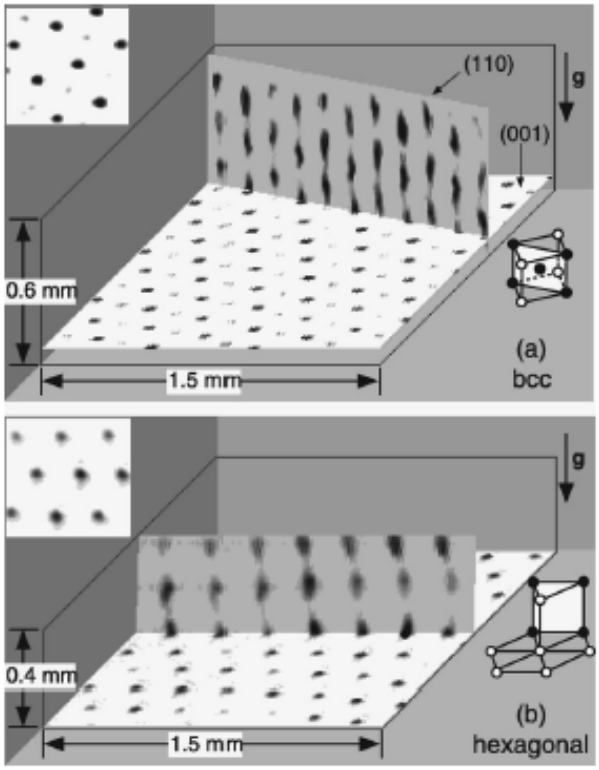

Figure 11: Images within a 3-D volume of the coulomb crystal formed by 9.4 μm diam polymer spheres in a 190 Pa discharge. In each image one horizontal plane and a vertical cross section through the data are shown; the inset shows a portion of the horizontal plane viewed from above. The data are contained in a stack of horizontal planar images resolved by selective illumination by a 90 μm thick sheet of light from a focused, swept laser beam. The particle images appear longer in the vertical direction due to the infinite thickness of the laser sheet.

the gas pressure. Both structural and dynamical properties of the plasma crystal are determined (correlation functions, thermal and systematic particle motion, diffusion, viscosity, and interaction cross sections). From these examinations the following states are identified during the melting transition (compare also Figs. 10, 11, 12):

- "Crystalline," characterized by hexagonal horizontal lattice structure and vertical alignment, and few lattice defects.
- "Flow and floe," characterized by the coexistence of islands of ordered crystalline structure (floes) and systematic directed particle motion (flows). Thermal motion corresponds to room temperature ($v_{th} = 0.2 mm/s$) - directed flow velocities are typically half this. Translational and orientational order have decreased significantly, occasional vertical particle migration to other lattice plane is observed (see Fig. 12(a,b)).
- "Vibrational," characterized by a return to a more orientationally ordered structure and diminishing flow-regions. Vibrational amplitudes, thermal energy, and vertical migration of particles increase. The

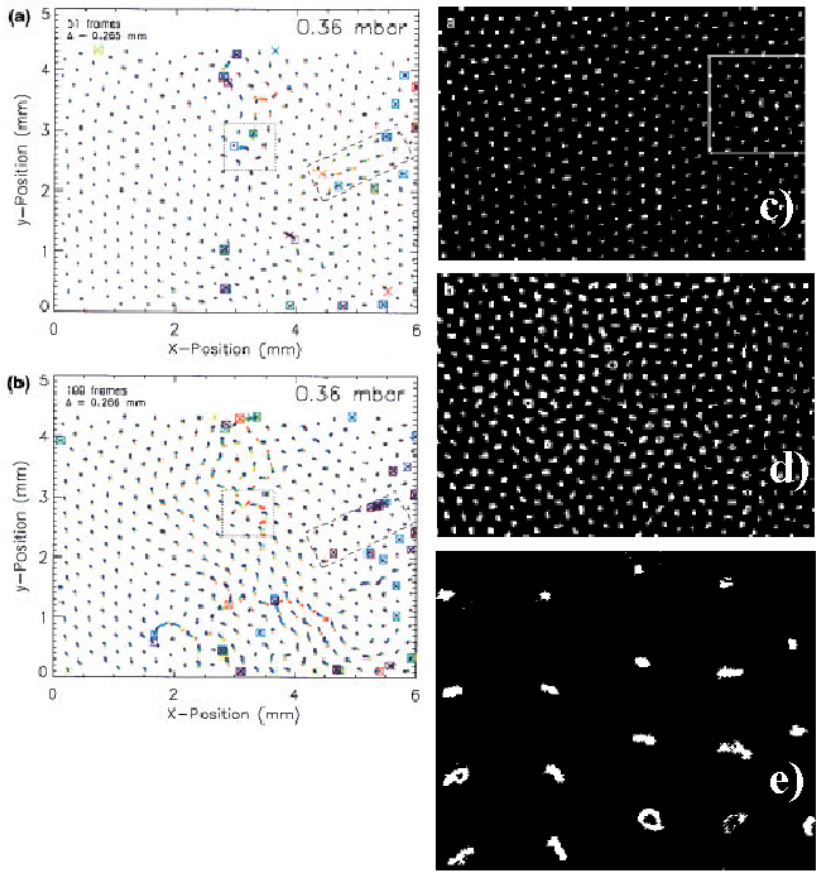

Figure 12:
Colour coded particle trajectories for two consecutive sequences (51 and 100 video frames respectively) at a neutral gas pressure of 0.36 mbar. The trajectories start with "red" and end with "violet." The coexistence of directed flows and stable regions are clearly seen. In the marked window (dotted lines) of (a) a new particle is seen to appear (blue square) leading to the displacement of the surrounding particles. In the second window (dashed lines) a particle disappears at the beginning of the sequence (red cross). The particles to the right move toward the newly formed dislocation to restore the structure. This motion influences particles as far as about six lattice distances. A reverse flow occurred in the lattice line above the latter. Also, some out-of-plane oscillations (superposed squares and crosses) mark the activity in this area. In (b), the particles from the dotted window exhibit an "eddy-like" flow pattern, whereas those in the dashed window are now stationary and highly ordered. Thus unstable regions (e.g., due to vertical particle migration) may stabilize as a result of ordered flows.

(c,d) The original images (three consecutive video frames overlayed) of the beginning and end of the vibrational state at pressures of 0.32 mbar (c) and 0.29 mbar (d). In the marked window in (c) the vibrations are first observed, then they spread throughout the "crystal".

(e) The side view of the plasma crystal in the vibrational state. This figure illustrates that the vibrations of the particles are essentially isotropic. Longer time observations confirm this, as well as statistical analyzes. Melting appears to start at the bottom of the crystal; the top surface remains frozen longest. From [18].

translational order continues to decrease (see Figs. 12(c,d)).

- "Disordered," characterized by collisions, complete vertical as well as horizontal migration. At this stage

Figure 13: Particle trajectories in the upper layer of the dust crystal with point defects and dislocations.

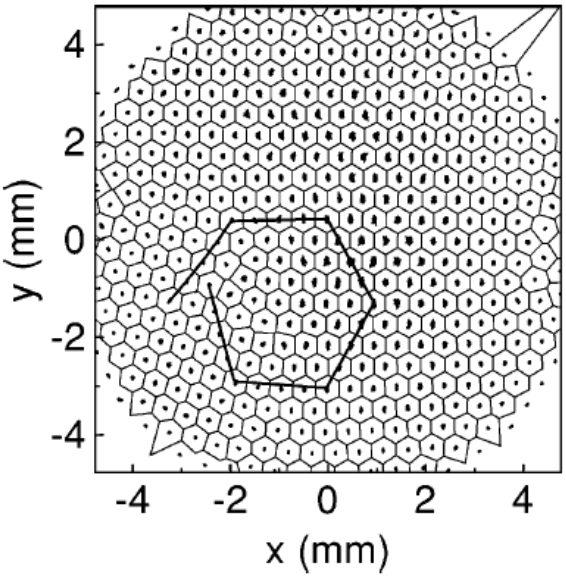

Figure 14: Scheme of the bilayer crystal with strong defects: the top incomplete layer (1), the upper lattice layer (2), the lower lattice layer (3), and bottom incomplete layer (4).

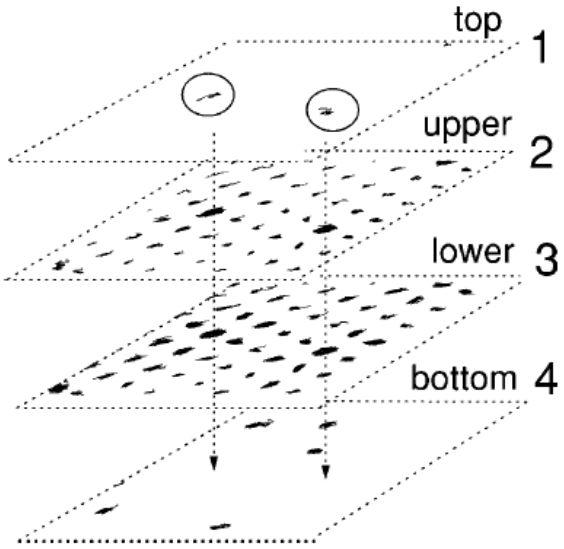

there is no discernible translational or orientational order, the thermal energy increases to $\approx 200\times$ room temperature, and Γ is of the order unity or less.

The unexpected vibrational phase, with its enhanced orientational order, might arise as the consequence of the mixed two- and three- dimensional nature of the flat plasma crystals. Alternatively, it may indicate the existence of a new intermediate state in melting transitions more generally.

It appears that properties of two-dimensional melting differ a lot from those of three-dimensional melting, as in common phase systems. While in 2D crystal particles form hexagonal and vertically aligned structure rather than close-packed, in 3D particles form standard fco structures. The melting transition in 2D is consisting of two steps, while in 3D it is somehow more complex.

To summarize, the transition appears to develop through the growth of crystal defects, directed particle flows around crystalline islands, enhanced vibrations associated with greater order and flow suppression, to a completely disordered state. This seems neither a straightforward first nor second order transition.

2.8 Melting of bilayer crystals with defect

[19]

The role of defects in the melting transition of a bilayer dust plasma crystal has also been studied. Two types of defects are considered:

- point defects and dislocations (Fig. 13) and
- additional particles that are placed below and above the bilayer crystal (*strong* defects, Fig. 14).

Bilayer crystal with point defects and uncorrelated dislocations exhibits a two-step melting dynamics: the instability is induced by decreasing gas friction and leads to the quick rise of the kinetic energy of particle motion. After transition to the hot crystalline regime with strong oscillations, system undergoes a melting

transition. Hence, the presence of point defects does not change the two-step melting scenario previously found for nondefect bilayer crystals. This contrasts with the influence of strong defects that imply more complex mechanism: global heating by self exited oscillations and the local heating by strong effects, which lead to a substantial increase of the kinetic energy of particles and to local heating of the bilayer dust crystal.

2.9 Gravitation limits the structure

The strong gravitational field at the Earth's surface restricts the formation of a plasma crystal in a device to a few lattice planes and may lead to inhomogeneities. The lattice collapses to the bottom of the device if the gravitational energy, $m_d gl$ (l is the scale length of the plasma, proportional to interparticle distance d or Debye screening length λ_D) is greater than the coulomb energy $\frac{q^2}{4\pi\epsilon_0 d}\exp(d/\lambda_D)$. These conditions set an upper limit for the particle size and a lower limit for N. If the experiment is done under no gravity, there is no limitation on the particle size. The lattice having a large lattice constant can be made in low-density plasma such as interplanetary plasma because q is proportional to a (connected with the capacitance) and $\Gamma \propto q^2 N^{1/3}$ so that the lower limit of N satisfying the solidification condition is proportional to a^{-6}.

The purpose of performing the space experiment under microgravity [5] was to study the possibility of the existence plasma-dust structures in the upper layer of the Earth's atmosphere when the particles are charged by a solar radiation as a result of the photoemission of electrons from their surface. Experimental investigations of the behaviour of an ensemble of macroparticles charged by solar radiation were performed under microgravitational conditions on board the Mir space station [20] , but there were no strong correlation between the interparticle distances be observed in spite of high particle charges and the large value of the coupling parameter.

3 Experimental advantages

- **Solid vs. plasma crystals** We have learnt that the main experimental advantage of plasma crystal over solid crystal is the possibility of visually following the processes in details. Moreover, plasma solids are easier to study theoretically too because the form of interaction potential is known. Of course, the theory of solid state has been developing for a century, while the theory of plasma dust crystal is still not quite consistent. Furthermore, the solid system is a quantum system and hence comparison is limited to a certain extent of classical or quasi-classical behaviour. However, it seems that quantum behaviour is not a serious obstacle, concerning some successful theories of melting [13].

- **Colloid vs. plasma crystals**

  While colloid and dust crystals share some basic properties, the experimental availability of the dust crystals is somehow superior.

  Both are overall charge-neutral systems and utilize small (colloidal) particles embedded in a partially ionized medium to organize and visualize structures produced by coulomb interactions.

  Unique properties of plasma crystals are very fast response times (million times shorter than colloidal crystal)[6], very little damping (again about $10^6\times$ less), easy experimental control, detailed imaging and high time resolution of the dynamics of individual particles, both in 2D and 3D. That makes plasma dust crystals handy for a large range of fundamental investigations into the liquid, plastic, and crystalline states to be conducted.

[5] Any object in freefall experiences microgravity conditions. Brief periods of microgravity can be achieved on Earth by dropping objects from tall structures. Longer periods are created through the use of airplanes, rockets, and spacecrafts. The microgravity environment associated with the space shuttle is a result of the spacecraft being in orbit, which is a state of continuous freefall around the Earth. The microgravity environment gives researches a unique opportunity to study the states of matter and the forces that affect them.

[6] However the presence of strongly coupled dust increases plasma time scales - the plasma reacts more slowly. It appears that the response time is fairly perfect for our examination facilities

Conclusion

As a progress in revealing and explaining three dimensional phenomena has also been made (for example, using Mie-scattering ellipsometry [21]), the consistency in theoretical explanation is still lacking. The interested reader may consult [7] for references. For example, simulations imply [22] that the stability of a hexagonal dust crystal depends strongly upon the gas neutral pressure; if the dust-neutral collision frequency is high enough, the ion flow will excite crystal waves (phonons) where the amplitude of these waves grows as a function of time and the crystal melts. Shortly, the instability waves in structure seem to be the major cause for melting transition in both two and three dimensions. Interestingly, the coexistence of the close-packed and fco structure has been observed [21].

The presence of dust particles in plasma adds new degrees of freedom to the system and generates many new ordered and disordered phenomena for many interesting studies. Recent research implies that the crystallization in dusty plasma can be a decent model for solid state phenomena.

However, it is not only theoretical insight that makes dust crystals research useful. Dust plasma crystals as well as common dusty plasma can contaminate material surface in technological processing, so it would be beneficial to find out how it could be prevented. On the other hand, crystal structures as fullerenes can be grown; a few grams of fullerenes can be produced in one our in a plasma and the process can be applied to industrial production of fullerenes C_{60} [23, 24]. Fullerenes were discovered in an attempt to recreate the conditions believed to exist in interstellar clouds. Among fullerenes, nanotubes and nanoparticles can also be created from dust in plasma [25]. These nanostructures are not plasma crystals by our definition, yet the possibility to form similar larger structures in the form of macroscopic crystals is quite attractive.

References

[1] B. Kmetec, "Prašna plazma." This introduction can be downloaded from http://kgb.ijs.si/ f4/seminar/files/2001_2002/dusty.pdf., December 2001. 1, 2.1

[2] J. Maddox, "Plasma dust as model crystals," *Nature*, vol. 370, no. 6489, p. 411, 1994. 1.1

[3] A. Piel, "Plasma crystals show new order," *Physics World*, vol. 7, no. 10, p. 23, 1994. 1.1

[4] H. Thomas and G. Morfill, "Melting dynamics of a plasma crystal," *Nature*, vol. 379, no. 6568, p. 806, 1996. 1.1

[5] D. G. Grier, "On the points of melting," *Nature*, vol. 379, no. 6568, p. 773, 1996. 1.1

[6] V. Tsytovich, "Dust plasma crystals, drops and clouds," *Physics-Uspekhi*, vol. 40, no. 1, p. 53, 1997. 1.1

[7] A. Piel and A. Melzer, "Dynamical properties in complex plasmas," *Plasma Phys. Control. Fusion*, vol. 44, p. R1, 2002. 2.1, 3

[8] A. Bouchoule, *Dusty plasmas*. John Wiley and sons, 1999. 2.1

[9] H. Ikezi, "Coulomb solid of small particles in plasmas," *Phys. Fluids*, vol. 29, no. 6, p. 1764, 1986. 2.1, 1

[10] F. F. Chen, *Plasma Physics*. Plenum Press, I Edition 1974, II Edition 1984. 2.1

[11] H. Thomas, G. Morfill, and V. Demmel, "Plasma crystal: Coulomb crystallization in a dusty plasma," *Phys. Rev. Lett.*, vol. 73, no. 5, p. 652, 1994. 2.2, 2, 3, 2.7

[12] J. H. Chu and I. Lin, "Direct observation of coulomb crystals and liquids in strongly coupled rf dusty plasma," *Physical Review Letters*, vol. 72, no. 25, p. 4009, 1994. 4, 2.3

[13] A. Melzer, A. Homann, and A. Piel, "Experimental investigation of the melting transition of the plasma crystal," *Phys. Rev. E*, vol. 53, no. 3, p. 2757, 1996. 2.4, 5, 3, 3

[14] A. Melzer, V. A. Schweigert, I. V. Schweigert, A. Homann, S. Peters, and A. Piel, "Structure and stability of the plasma crystal," *Physical Rev. E*, vol. 54, no. 1, p. R46, 1996. 4

[15] V. A. Schweigert, I. Schweigert, A. Melzer, A. Homann, and A. Piel, "Plasma crystal melting: A nonequilibrium phase transition," *Physical Rev. Letters*, vol. 80, no. 24, p. 5345, 1998. 6

[16] V. A. Schweigert, I. Schweigert, A. Melzer, A. Homann, and A. Piel, "Alignment and instability of dust crystals in plasmas," *Physical Review E*, vol. 54, no. 4, p. 4155, 1996. 7, 8

[17] S.Hamaguchi, R. T. Farouki, and D. H. E. Dubin, "Triple point of Yukawa systems," *Physical Rev. E*, vol. 56, no. 4, p. 4671, 1997. 2.6, 9

[18] G. E. Morfill, H. M. Thomas, U. Konopka, and M. Zuzic, "The plasma condensation: Liquid and crystalline plasmas," *Physics of Plasmas*, vol. 6, no. 5, p. 1769, 1999. 12

[19] I. V. Schweigert, V. A. Schweigert, A.Melzer, and A.Piel, "Melting of dust plasma crystals with defects," *Physical Review E*, vol. 62, no. 1, p. 62, 2000. 2.8

[20] V.E.Fortov, V.I.Molotkov, A.P.Nefedov, and O.F.Petrov, "Liquid- and crystalline structures in strongly coupled dusty plasmas," *Physics of Plasmas*, vol. 6, no. 5, p. 1759, 1999. 5

[21] Y. Hayashi, "Structure of a three-dimensional coulomb crystal in a fine-particle plasma," *Phys. Rev. Lett.*, vol. 83, no. 23, p. 4764, 1999. 3

[22] F. Melandsø, "Heating and phase transitions of dust-plasma crystals in a flowing plasma," *Phys. Rev. E*, vol. 55, no. 6, p. 7495, 1997. 3

[23] K. Yoshie and others., "Novel method for C_{60} synthesis: A thermal plasma at athmospheric pressure," *Appl. Phys. Lett.*, vol. 61, no. 23, p. 2782, 1992. 3

[24] D. Gruen, S. Liu, A. Krauss, and X. Pan, "Buckyball microwave plasmas: Fragmentation and diamond-film growth," *J. Appl. Phys.*, vol. 75, no. 3, p. 1758, 1994. 3

[25] A. Burden and R. Silva, "Fullerene and nanotube formation in cool terrestrial dusty plasmas," *Appl. phys. Lett.*, vol. 73, no. 21, p. 3082, 1998. 3